J. Phys. B: At. Mol. Opt. Phys. 24 (1991) 209–218. Printed in the UK

Transfer ionization in He^{2+}–H^- collisions: cross section measurements in the energy range 0.2–1300 eV

M H Cherkani, S Szücs, M Terao, H Hus and F Brouillard

Université Catholique de Louvain, Département de Physique, Unité de Physique Atomique et Moléculaire, chemin du cyclotron, 2, B 1348 Louvain-la-Neuve, Belgium

Received 12 June 1990, in final form 24 July 1990

Abstract. This paper reports on measurements of the cross section for transfer ionization in He^{2+}–H^- collisions over the barycentric energy range 0.16–1300 eV. The experimental method involves merged beams and coincident detection of the reaction products. The dependence of the cross section on the energy is rather similar to that of the one-electron exchange, suggesting that a two-step mechanism dominates the process.

1. Introduction

Two-electron processes in low energy collisions of multiply charged ions have received an increasing attention in the last years, both experimentally and theoretically (see, e.g. Salzborn and Müller 1986, Janev *et al* 1986). Experimentally, however, most of the work has dealt with many-electron systems. Such systems are not best suited to assess the validity of the theoretical approaches proposed for modelling the collision dynamics, as the comparison between experimental and theoretical results remains obscured by the additional approximations introduced to describe a complex system. From that point of view, experiments with simple systems and particularly with two-electron systems are preferable.

The present work deals with such a system. It is devoted to the measurement of the cross section for transfer ionization in collisions of H^- with H^{2+}

$$H^- + He^{2+} \rightarrow H^+ + He^+ + e.$$

It is the first study of transfer ionization in this collisional system that can be regarded as a prototype of multiply charged ion–atom collisions. To our knowledge, the only other study of transfer ionization in a two-electron system is that published by Schön *et al* (1987).

The present measurements have been carried out using the unambiguous experimental method consisting in the coincident detection of H^+ and He^+ ions formed in the interaction of merged H^- and He^{2+} beams.

2. Apparatus and experimental method

The He^{2+} and H^- beams are extracted from their sources, a multicusp and a duoplasmatron source respectively, accelerated by independent voltages (some 10 kV),

0953-4075/91/010209+10$03.50

momentum analysed and focused in the standard fashion. They are deflected electrostatically so as to pass through a common diaphragm O (6 mm diameter) centred on the final merging axis, crossing this axis under the same but opposite angle of 5°. Diaphragm O is taken as the starting point of the present description of the apparatus, which is shown schematically in figure 1.

A second set of diaphragms O_1 (1 mm diameter) and O_2 (2 mm diameter), located some 15 cm behind O, define the sections of the H^- and He^{2+} beams respectively. The size of these diaphragms is small compared with the diameter of the beams, which is of the order of 10 mm (width at half maximum). The current densities in the transmitted beams can therefore be regarded as essentially constant over the beam sections. In addition care is taken to collimate the beams, thus reducing their divergence to the minimum determined by their emittance. In fact this divergence is of the order 1.7 mrad (half angle). Immediately after their passage through O_1 and O_2 (entrance of the high vacuum chamber) the beams are bent towards the axis by a pair of electrostatic deflectors M_1 and M_2 and then merged (on the final axis) by a third common deflector M.

The 'observation cell' (C) is made of a series of 11 plates perpendicular to the axis, with 7 mm diameter holes precisely centred on the merging axis. This enables one to establish a controlled potential on the axis. The purpose of this potential is to delimit the length over which the beams usefully interact. By usefully, we mean that the reaction products can reach their detectors, i.e. they have the right kinetic energy to pass the magnetic analyser (B). As the kinetic energy of the reaction products is related to the potential at the reaction site, it is therefore possible to restrict the observation to those reactions taking place at the potential of the observation cell.

The division of the observation cell into 11 electrodes makes it possible to vary the effective interaction length. It also provides the possibility of working with non-uniform potentials inside the observation cell and so improving the time resolution in coincident measurements as discussed below. It must be pointed out that the observation potential also modifies the collision energy and is in fact used to control this energy. If the collision cell is biased to some observation voltage V the CM energy E_R of the

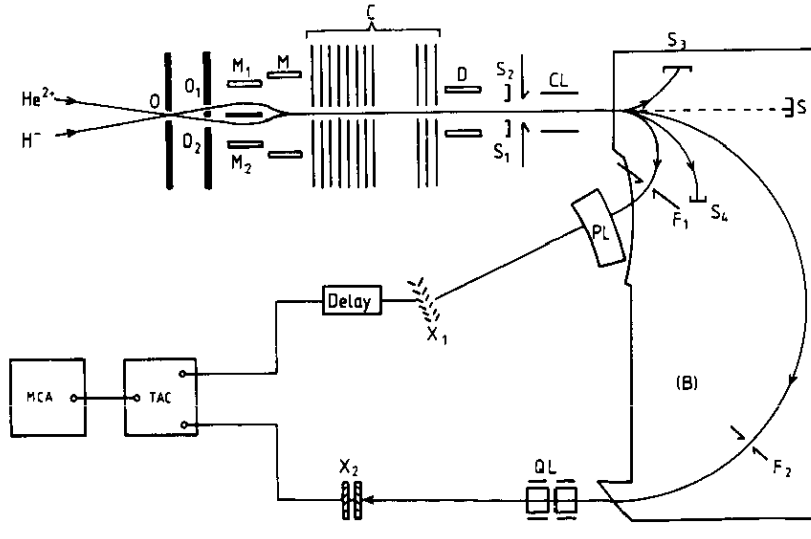

Figure 1. Schematic diagram of the apparatus.

collision is:

$$E_R\,(\mathrm{eV}) = \mu\left[\left(\frac{20.000-2V}{m_2}\right)^{1/2}-\left(\frac{10.000+V}{m_1}\right)^{1/2}\right]^2$$

where m_1 and m_2 are the masses of H^- and He^{2+} respectively (in amu) and $\mu = m_1m_2/m_1+m_2$ is their reduced mass (in amu).

The exact merging of the beams is achieved using the following procedure. For a set of values of the voltage on the common deflector M, the corresponding values of the voltage on the deflector M_1 (or M_2) are determined by requiring the $H^-(He^{2+})$ beam to reach a small probe S located some 110 cm behind the centre of the observation cell. For each value of the voltage on M with the corresponding voltages on M_1 and M_2, the offset of the H^- and He^{2+} with respect to the merging axis is measured by sliding the third plate of the observation cell (movable on a micrometric device) to progressively intercept the beams. Simultaneously, the transmitted intensities are recorded on the probes S_1 and S_2 on which the H^- and He^{2+} beams are respectively deflected by means of the demerging deflector D. The right voltage to be applied on M is the one giving the same offset to the two beams. This offset must of course be small (as a rule, a maximum of 0.05 mm was imposed). Whenever a larger offset was observed, the direction of the beams were readjusted prior to their entrance to the merging section.

After the observation cell, the beams are passed through a magnetic analyser (B). The primary beams H^- and He^{2+} are collected on probes S_3 and S_4, situated in the magnetic field and thus not liable to secondary emission, and their intensities measured by means of electrometers. The reaction products H^+ and He^+ with energy corresponding to their formation in the observation cell, are filtered by the slits F_1 and F_2 respectively and detected by means of electron multipliers X_1 and X_2.

The collection of the ions scattered off the axis is insured by inserting three electrostatic lenses that complete the focusing action of the magnetic analyser: a cylindrical lens (CL) that collimates the H^+ beam in view of its focusing on the slit F_1, a prismatic lens (PL) that provides the vertical focusing of the H^+ beam, a set of quadrupoles lenses (QL) for the focusing of the He^+ beam. The angular acceptances determined by this focusing configuration are 20 mrad and 80 mrad for H^+ and He^+ respectively. They are approximately inversely proportional to the masses and therefore well matched. In terms of the centre-of-mass scattering angle this corresponds to an acceptance of 20° at 1 keV and 60° at zero CM energy (this last value is obtained assuming for the reaction an exothermicity of 6 eV).

The signals from the electron multiplier detectors are time analysed to extract the time correlated pairs produced by the transfer ionization reactions out of the uncorrelated signals created by the interaction of the beams with the residual gas. This is achieved using a time-to-amplitude converter. The signals from the detectors are fed into the start and the stop inputs of the converter. A multichannel pulse height analyser then records the number of ion pairs detected as a function of the time lag between them. The products of transfer ionization appear with a definite lag corresponding to the difference in their times of flight, which is slightly spread by the length of the observation cell. They therefore build up a characteristic peak in the spectrum above the flat background associated with the detection of uncorrelated He^+ and H^+ ions formed in the interaction of the beams with the residual gas in the observation cell (as shown in figure 3(*a*)). The level of this background depends on the pressure in the observation cell. This pressure was always kept below 10^{-10} Torr.

For a complete collection of the product ions, the positions of the slits F_1 and F_2 must be adjusted according to the kinetic energies of these ions. These energies are affected by the unknown exothermicity of the transfer ionization process which has a considerable effect because of the well known kinematic amplification associated with merged beams. They must therefore be determined experimentally. This is achieved by observing both the total He^+ count rate and the (coincident) signal as a function of the field of the magnetic analyser. The total count rate is recorded first, having fixed the position of the slit F_2. The value of the field at the centre of the peak (full triangles in figure 2) corresponds to the energy of He^+ ions formed on residual gas in the observation cell. The exothermicity of this process is of little influence on the energy of the ion as it is not kinematically amplified. With this value of the field, the position of the slit F_1 is adjusted for a maximum of the H^+ counting rate, thus properly collecting the protons formed in the interaction of H^- with the residual gas. Then the magnetic field is varied step by step and the rate of He^+-H^+ coincidences is recorded at each step. For each measurement, the position of slit F_1 is readjusted, although it is a wide slit (4 mm), to ensure that it corresponds to the energy of an H^+ formed by transfer ionization together with an He^+ ion passing the slit F_2. The necessary adjustment is easily calculated, considering that the exothermicity of the reaction produces equal variations of the momenta of He^+ and H^+. In this way, a second curve is obtained (open squares in figure 2) substantially shifted from the first one, towards higher or lower field values depending on whether the He^{2+} ion is faster or slower than the H^- ion. In the case reported in figure 2, the shift is about 6 G, corresponding to an energy shift of 180 eV. The centre of the shifted peak determines both the field value and the position of the slit F_1 that are used in the transfer ionization cross section measurements.

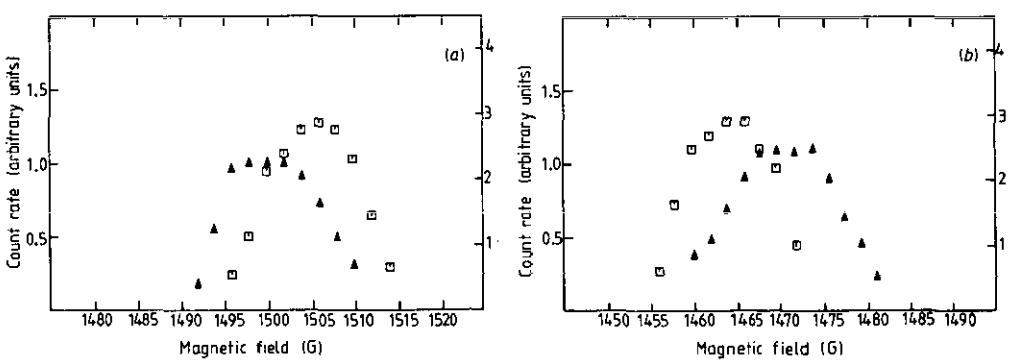

Figure 2. Measurement of the shifts in energy of He^+ produced in the transfer ionization reaction (□, signal) and in the interaction of the He^{2+} beam with residual gas (▲ background). $E_R = 10$ eV. (*a*) He^{2+} faster than H^-, (*b*) He^{2+} slower than H^-.

The rate of transfer ionization is obtained from the time lag spectrum (figure 3) by subtracting the area of the background under the peak from its total area. This background area is taken approximately to be the mean value of the background in the vicinity of the peak. The importance of the background contribution is obviously related to the width (τ) of the signal, i.e. to the spread of the time lag separating the detection of He^+ and H^+. The signal-to-background ratio will therefore be enhanced if this spread is reduced. The spread is for the largest part due to the length (l) of the observation cell: reactions taking place near the entrance of the cell lead to larger

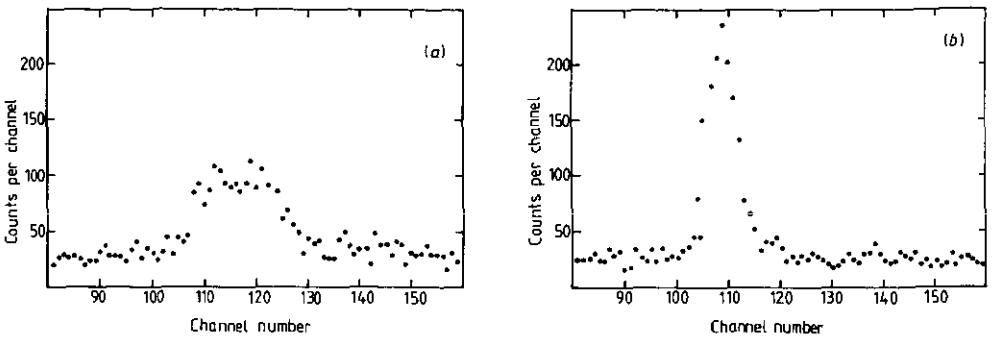

Figure 3. Example of a time lag coincidence spectrum: (*a*) $\Delta V = 0$, unbunched spectrum; (*b*) $\Delta V \neq 0$ bunched spectrum.

times of flight than reactions occurring near the exit. Reducing (l) reduces the spread but reduces the signal as well. One way to lower the spread without reducing (l) is to apply a non-uniform voltage to the observation cell. A non-uniform voltage will result for the product ions in a final velocity depending on the position of the reaction site in the cell. It can be chosen such that the time lag becomes position independent, performing a sort of 'bunching' of the time lags. The time lag between H^+ and He^+ is given by

$$\Delta t(x) = \left(\frac{x}{v_1} - \frac{x}{v_2}\right) + \left(\frac{L_1}{v_1'} - \frac{L_2}{v_2'}\right).$$

The first term on the right side represents the time lag in the observation cell, x being the flight length in this cell of H^+ and He^+ with their velocities v_1 and v_2. The second term is the time lag between H^+ and He^+ outside the observation cell, L_1, L_2, v_1' and v_2' being the flight lengths and the velocities of H^+ and He^+ outside the observation cell. The velocities v_1, v_2, v_1' and v_2' are functions of the observation voltage V and thus of the position x of the reaction site. If we choose a voltage with linear variation:

$$V(x) = V + (x/l)\Delta V$$

we can determine the value of ΔV (bunching voltage) from the bunching condition:

$$\frac{\mathrm{d}}{\mathrm{d}x}\Delta t(x) = 0.$$

The bunching effect of this non uniform potential is shown in figure 4, where the width

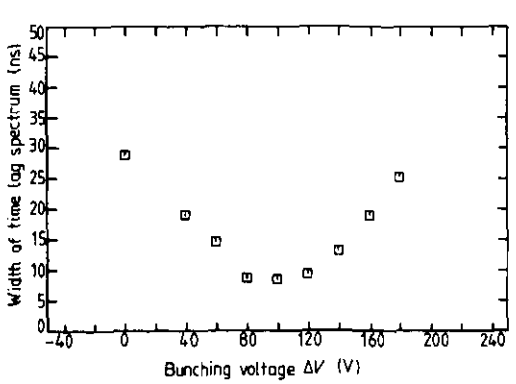

Figure 4. Width of the time lag coincidence peak as a function of the bunching voltage ΔV for $D^- + {}^3He^{2+}$. $V_0 = -2680$ V, $E_R = 1250$ eV.

of the lag spectrum is given as a function of ΔV and in figure 3 where we compare a bunched and a unbunched time lag spectrum. This non-uniform potential will of course affect the collision energy but the relative energy spread introduced by this potential is small (of the order of $l/(L_1+L_2)$).

The cross section for transfer ionization is derived from the observed signal through the relation:

$$\sigma = \frac{N}{\eta_1 \eta_2} \frac{v_1 v_2}{|v_1 - v_2|} \frac{2e^2}{\int I_1 I_2 \, dt} \frac{s}{l} \gamma.$$

N is the number of $(H^+\text{-}He^+)$ ion pairs recorded during the measurement. v_1 and v_2 are the velocities of H^- and He^{2+} inside the observation cell. I_1 and I_2 are the intensities of the H^- and He^{2+} beams as measured on S_3 and S_4. η_1 and η_2 are the efficiencies of the H^+ and He^+ detectors, an EMI electron multiplier and a pair of channelplates respectively. Their values $\eta_1 = 98\% \pm 2\%$ and $\eta_2 = 60\% \pm 5\%$ are determined as described in previous work (Szücs *et al* 1984, Terao *et al* 1986). l is the interaction length. Its value here is 78 ± 2 mm, and is determined by the axial distribution of the observation voltage and by the energy resolutions of the slits F_1 and F_2. s is the section of the He^{2+} beam, as defined by the diaphragm O_2 (diameter 2 mm). γ is a correction factor for the lens effect occurring at the entrance of the observation cell and that slightly modifies the sections of the interacting beams.

Table 1. Systematic uncertainties in σ.

		Uncertainties at the relative energy				
Parameter	E_R (eV) = 0.3	1	10	100	1000
Detection efficiency					
EMI(H^+) η_1			±2%		
Channel plates (He^+) η_2			±5%		
Interaction length l			±3%		
Beam intensity $^3He^{2+}$ and H^- I_1 and I_2			±1%		
Relative velocity v_R	20%	6%	1.6%	0.5%	0.3%
Background subtraction (statistical error)	5%	5%	4%	4%	2%
Quadrature sum	22%	10%	8%	8%	7%

Table 2. Typical operating parameters for $H^- + He^{2+} \rightarrow H^+ + He^+ + e^-$ at $E_R = 64$ eV.

Primary beam intensities:		H^- 200 nA at 10 keV
		He^{2+} 20 nA at 20 keV
Observation voltage:		$V = -1000$ V
Count rate:	background	He^+ 6000 Hz
		H^+ 4000 Hz
		Random coincidences = 0.5 Hz
	signal	2 Hz
Width of time lag spectrum		<10 ns
Measurement time for 5% statistical error: (90% confidence level)		16 min
Vacuum in the collision chamber		$<10^{-10}$ Torr

The integration of the product $I_1 I_2$, over the measurement time, is continuously carried out by means of an analogue multiplier followed by a voltage-to-frequency converter and a scaler.

The uncertainties in the different quantities involved in the calculation of the cross section are presented in table 1. The uncertainty in the relative velocity $v_R = |v_1 - v_2|$ mainly results from the residual beam divergence (emittance). This divergence shifts the CM energy by a small amount of the order of 0.05 eV which is taken into account but it also spreads it by about 0.1 eV. This spread is the origin of the uncertainty on v_R. The uncertainties in v_1 and v_2 associated with the limited resolution of the beam energies are negligible.

3. Results and comments

The values obtained for the cross section of the transfer ionization

$$H^- + He^{2+} \rightarrow H^+ + He^+ + e$$

are displayed in figure 5.

To cover a wide range of relative velocity (from 7×10^6 to 6×10^7 cm s^{-1}), four isotope combinations were used in the measurements: $H^- + {}^3He^{2+}$, $H^- + {}^4He^{2+}$, $D^- + {}^3He^{2+}$, $D^- + {}^4He^{2+}$. The relative velocity ranges covered with the different combinations

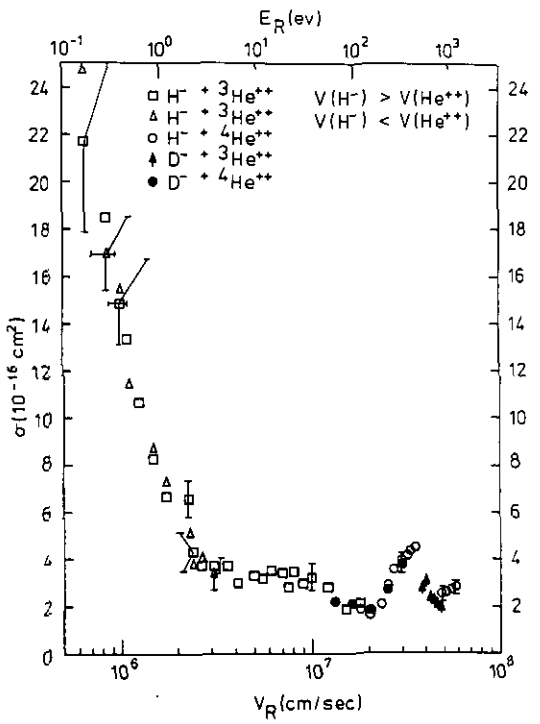

Figure 5. Transfer ionization cross section in $H^-(D^-) + {}^3He^{2+}({}^4He^{2+})$ collisions as a function of the relative velocity. The relative energy scale is for the $H^- + {}^3He^{2+}$ system. Vertical bars show the error estimated from the dispersion observed in the results. Horizontal bars denote the uncertainty in v_R.

have important overlaps. As can be seen, the measurements performed with different isotopes, thus in quite different experimental conditions, are in good agreement. Furthermore, an additional check was done on the $H^- + {}^3He^{2+}$ measurements, carrying them out in the two possible ways that a given relative velocity can be achieved with merged beams, i.e. with H^- faster or slower than He^{2+}. Here also an excellent agreement was found. This provides strong confidence in the reliability of the results. The final

Table 3. Experimental transfer ionization cross sections for $H^-(D^-) + {}^3He^{2+}({}^4He^{2+}) \rightarrow H^+(D^+) + {}^3He^+({}^4He^+) + e^-$.

V_R (10^6 cm s^{-1})	E_R (eV)	σ (10^{-16} cm^2)	$\pm\varepsilon$ (10^{-16} cm^2)
0.65	0.16	23.6	2.5
0.85	0.30	17.9	2.0
1.00	0.40	14.9	1.9
1.10	0.50	12.5	2.3
1.25	0.60	10.7	2.2
1.50	0.90	8.5	0.5
1.75	1.2	7.0	0.6
2.30	2.1	6.0	0.7
2.40	2.3	4.1	0.7
2.66	2.8	3.9	0.4
3.05	3.6	3.6	0.4
3.60	5.0	3.7	0.9
4.10	6.5	3.0	0.6
5.00	10.0	3.3	0.4
5.50	12.0	3.2	0.5
6.10	14.3	3.5	0.6
7.00	19.0	3.4	0.8
7.50	22.5	2.8	1.0
8.00	25.0	3.5	0.5
9.00	32.0	3.0	0.6
10.00	39.5	3.2	0.7
12.00	56.0	2.8	0.6
13.00	61.0	2.2	0.3
15.00	90.0	1.9	0.8
16.00	100.0	2.0	0.3
18.00	125.0	2.1	0.3
20.00	155.0	1.8	0.2
22.50	197.0	2.1	0.2
25.00	243.0	2.9	0.2
27.50	294.0	3.5	0.1
30.00	350.0	4.2	0.4
32.00	400.0	4.2	0.2
33.00	425.0	4.4	0.4
35.00	477.0	4.5	0.6
38.00	562.0	2.7	0.2
40.00	622.0	3.0	0.4
42.00	686.0	2.3	0.3
44.00	753.0	2.2	0.2
46.00	823.0	2.0	0.1
48.00	896.0	1.9	0.1
50.00	978.0	2.5	0.7
52.00	1050.0	2.6	0.4
54.00	1135.0	2.6	0.3
58.00	1308.0	2.8	0.3

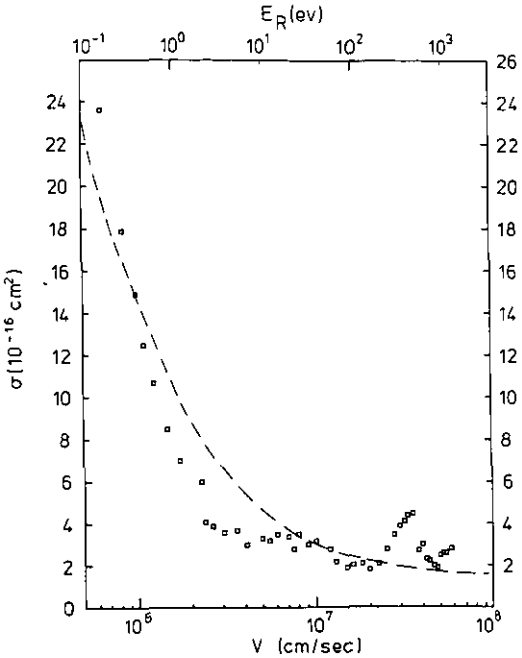

Figure 6. Transfer ionization cross section: □, experiment; – – –, calculation.

results, that incorporate all the measurements, are listed in table 3 and shown in figure 6. The error indicated in column 4 reports the dispersion observed in the results obtained in repeated measurements (about 10 measurements were taken for each energy). It thus contains all the errors of fluctuating nature. It is consistent with the estimations presented in table 1.

The cross section shows a $1/E$ dependence at low barycentric energy (below 5 eV), due to the effect of the Coulomb attraction (at these energies the relative velocity of the collidants is mainly determined by the Coulomb attraction of H^- and He^{2+}). At higher CM energy the energy dependence is very similar to that observed in the one-electron exchange (Terao *et al* 1986), showing two maxima at 25 and 400 eV. This suggests that the transfer ionization is dominated by a two-step mechanism:

$$H^- + He^{2+} \rightarrow H(1s) + He^+(n) \rightarrow H^+ + He^+ + e.$$

The broken curve shown in figure 6 is the result of a simple semiclassical (impact parameter) calculation performed with this view, where the probability of the first step is calculated in the Landau–Zener approximation and where the second step is treated as a resonant Penning ionization. Details on this calculation will be reported in another paper together with other experiments carried out to determine the final state of the He^+ product ion.

Acknowledgments

This work was performed with the support of the Institut Interuniversitaire des Sciences Nuclaires and of the Association Euratom-Etat Belge.

References

Janev R K, Lazur V Yu and Grozdanov T P 1986 *J. Phys. B: At. Mol. Phys.* **19** 421–36

Salzborn E and Müller A 1986 *Atomic Processes in Electron–Ion and Ion–Ion Collisions* Series B vol 45 ed F Brouillard (New York: NATO Advanced Study Institutes; Plenum) pp 357–402

Schön W, Krüdener S, Melchert F, Rinn K, Wagner M, Salzborn E, Karemera M, Szücs S, Terao M, Fussen D, Janev R K, Urbain X and Brouillard F 1987 *Phys. Rev. Lett.* **59** 1565

Szücs S, Karemera M, Terao M and Brouillard F 1984 *J. Phys. B: At. Mol. Phys.* **17** 1613

Terao M, Szücs S, Cherkani M, Brouillard F, Allan R J, Harel C and Salin A 1986 *Europhys. Lett.* **1** 123–8